CELL BIOLOGY

Dynamics and regulation of mitotic chromatin accessibility bookmarking at single-cell resolution

Qiaoni Yu[1,2,3†], Xu Liu[1,4†], Jingwen Fang[5,6†], Huihui Wu[1,4†], Chuang Guo[1], Wen Zhang[1], Nianping Liu[1], Chen Jiang[1], Qing Sha[1], Xiao Yuan[1,4], Zhikai Wang[1,4,5*], Kun Qu[1,2,3,5*]

Although mitotic chromosomes are highly compacted and transcriptionally inert, some active chromatin features are retained during mitosis to ensure the proper postmitotic reestablishment of maternal transcriptional programs, a phenomenon termed "mitotic bookmarking." However, the dynamics and regulation of mitotic bookmarking have not been systemically surveyed. Using single-cell transposase-accessible chromatin sequencing (scATAC-seq), we examined 6538 mitotic L02 human liver cells of variable stages and found that chromatin accessibility remained changing throughout cell division, with a constant decrease until metaphase and a gradual increase as chromosomes segregated. In particular, a subset of chromatin regions were identified to remain open throughout mitosis, and genes associated with these bookmarked regions are primarily linked to rapid reactivation upon mitotic exit. We also demonstrated that nuclear transcription factor Y subunit α (NF-YA) preferentially occupied bookmarked regions and contributed to transcriptional reactivation after mitosis. Our study uncovers the dynamic and regulatory blueprint of mitotic bookmarking.

INTRODUCTION

Mitosis is concomitant with global histone phosphorylation and deacetylation (*1*), the loss of chromatin accessibility and long-range chromatin interactions (*2*), and the dissociation of RNA polymerase II (Pol II) and transcription factors (TFs) from chromatin (*3*, *4*), resulting in the silencing of gene transcription. Despite this, emerging observations have indicated that some chromatin features are partially or completely preserved during mitosis, conveying gene regulatory architectures like "bookmarks," which is known as "mitotic bookmarking." These bookmarking factors include DNA methylation (*5*), histone modifications (*6*, *7*), the accessibility of specific chromatin regulatory regions (*8*), and the binding of general and sequence-specific TFs (*9*–*14*). Among those, chromatin accessibility bookmarking directly associated with TF binding (*15*) is globally maintained during mitosis, especially at promoters, which ensures that mitotic chromatin can be accessed by bookmarking TFs (*8*, *14*). Therefore, retention of chromatin accessibility bookmarking is considered to be essential for the regulation of transcriptional reactivation after mitosis. Collectively, the structural and functional states of active genes could be bookmarked to ensure their proper reactivation after mitosis (*16*), which is essential for the transmission of transcriptional memory from mother cells to daughter progenies (*17*).

Mitotic bookmarking is influenced by chromosome condensation, which is highly dynamic at different stages of mitosis (*18*). In addition, several studies have shown that some epigenetic signatures previously considered as bookmarking factors (*7*) were not consistently retained on chromatin throughout mitosis (*19*, *20*). Thus, it is limiting to study the bookmarking using drug-synchronized mitotic cells. One drug widely used for mitotic cell enrichment is nocodazole, a small molecule that inhibits spindle microtubule assembly. Nocodazole treatment not only synchronizes cells specifically at prometaphase but also can cause contamination problems as remnant interphase cells detach from the petri dish (*21*), which may compromise the exploration of mitotic bookmarking. Recent studies have used single-cell sequencing technologies to investigate the variabilities of chromosome organization (*22*), transcriptomes (*23*), and proteomes (*24*) that are present throughout the entire cell cycle, thus providing an empirical basis for dissecting the dynamics of mitotic bookmarking.

Here, using the plate-based single-cell transposase-accessible chromatin sequencing (scATAC-seq) technique (*25*), we analyzed 6538 mitotic cells and characterized the dynamics of chromatin accessibility during mitosis. We showed that chromatin accessibility continued to decrease after mitotic entry and then began to increase at the metaphase-anaphase transition. This dynamic bookmarking map presented a subset of chromatin regions that remained open throughout mitosis known as bookmarked regions. These regions were enriched in promoters of genes that were rapidly reactivated after mitosis. We further demonstrated that nuclear transcription factor Y subunit α (NF-YA) functioned as a bookmarking TF by preferentially occupying the bookmarked regions, and NF-YA knockdown (KD) impaired chromatin accessibility expansion and transcriptional reactivation upon mitotic exit. Together, our study identifies the bookmarked chromatin regions from highly dynamic chromatin accessibility and highlights the bookmarking role of NF-YA in the reestablishment of chromatin and transcription in daughter cells.

[1]MOE Key Laboratory for Cellular Dynamics, School of Basic Medical Sciences, Division of Life Sciences and Medicine, University of Science and Technology of China, Hefei 230027, China. [2]Institute of Artificial Intelligence, Hefei Comprehensive National Science Center, Hefei 230088, China. [3]Department of Oncology, The First Affiliated Hospital of USTC, Division of Life Sciences and Medicine, University of Science and Technology of China, Hefei 230021, China. [4]Keck Center for Organoids Plasticity, Morehouse School of Medicine, Atlanta, GA, USA. [5]Hefei National Research Center for Physical Sciences at the Microscale, University of Science and Technology of China, Hefei 230026, China. [6]HanGene Biotech, Xiaoshan Innovation Polis, Hangzhou, Zhejiang 311200, China.
†These authors contributed equally to this work.
*Corresponding author. Email: qukun@ustc.edu.cn (K.Q.); wangzk@ustc.edu.cn (Z. W.)

RESULTS

Dynamic changes in chromatin accessibility during mitosis

To investigate the dynamics of chromatin accessibility during mitotic cell division, we performed scATAC-seq analysis for unsynchronized mitotic L02 human liver cells that were sorted by flow cytometry based on the signal of histone H3 phosphorylation at serine 10 (H3pS10), a mitosis-specific marker (Fig. 1A; see Materials and Methods) (*6*, *26*). Mitotic purity was verified by immunofluorescence imaging, which also showed that the fluorescence-activated cell sorting (FACS)–sorted unsynchronized H3pS10-positive ($H3pS10^+$) population included cells in prophase, prometaphase, metaphase, and anaphase (fig. S1, A and B). Synchronized cells that were blocked in prophase (RO3306 treatment), metaphase (MG132 treatment), and anaphase (blebbistatin treatment) were also included in the analysis as time references for mitotic progression (fig. S1C). In total, 6538 cells with high-quality chromatin accessibility data were obtained (fig. S1, D and E), of which 5448 were unsynchronized $H3pS10^+$ cells, 352 were RO3306-treated prophase cells, 363 were MG132-treated metaphase cells, and 375 were blebbistatin-treated anaphase cells. For data analysis, the accessibility pattern-based epigenomic clustering (APEC) algorithm (*27*) was adopted for peak calling and identified a total of 30,671 accessible peaks in all cells. We then used Slingshot (*28*) to perform a pseudotime inference analysis and aligned these cells in a two-dimensional (2D) space (Fig. 1B).

The drug-synchronized prophase, metaphase, and anaphase cells were mainly distributed at the beginning, middle, and end of the trajectory, respectively (Fig. 1, C and D). In addition, the accessibility of *TAOK2* whose mRNA expression was reduced as mitosis progressed (*29*) decreased along the trajectory (Fig. 1E). In contrast, the locus of *TRIP13*, which is involved in the metaphase-anaphase transition checkpoint (*30*), was highly accessible at the end of the trajectory (Fig. 1F). These observations indicate that the mitotic trajectory defined in our pseudotime analysis effectively reflects the continuous mitotic cell progression from prophase to anaphase.

Notably, the chromatin accessibility of L02 cells continued to decrease by ~75% during the prophase-metaphase transition and began a gradual increase immediately after metaphase (Fig. 1G). To verify this, we performed image-based ATAC with visualization (ATAC-see) (*31*) to assess L02 cells at different mitotic phases (see Materials and Methods). We observed that chromatin accessibility gradually decreased after prophase and began to increase after reaching its nadir in metaphase (Fig. 1H), which is consistent with our scATAC-seq analysis and recent studies on the dynamics of active histone modifications of H3K27ac and H3K9ac during mitosis (*19*, *20*). Similar dynamic trends of mitotic chromatin accessibility were also observed in the other two cell lines (HepG2 and HUH7) by ATAC-see (fig. S1, F and G). These results suggest that chromatin accessibility decreases continually from mitotic entry until metaphase, when it begins to increase.

scATAC-seq analysis identifies mitotic bookmarked regions

Since pseudotime-aligned mitotic cells could faithfully represent the mitotic progression of one cell, as previously illustrated (*32*), chromatin accessibility analysis of the pseudotime-aligned cell population would be much more informative, although the profile of scATAC-seq presents a momentary snapshot of the cell's chromatin accessibility. Therefore, we ranked each cell according to its pseudotime and constructed a dynamic map of chromatin accessibility for all 30,671 peaks throughout mitosis (Fig. 2A). We counted the number of newly opened or closed chromatin regions at a specific pseudotime compared to the previous pseudotime. We found that the closing and opening events of the chromatin regions occurred continually before and after metaphase, respectively (fig. S2A), indicating that the condensation and decondensation of the genome during mitosis were both gradual processes. In sharp contrast to those chromatin regions that underwent dynamic closing and/or subsequent opening (i.e., unbookmarked regions), ~7% of the initially open chromatin regions ($n = 2249$) remained accessible throughout mitosis (Fig. 2, A and B), which, by definition, are the bookmarked regions. As a comparison, we performed bulk ATAC-seq analysis on unsynchronized and nocodazole-arrested L02 cells (fig. S2, B to E). Although 85% of the bookmarked regions were detectable in the bulk ATAC-seq analyses, 95% of the mitotic retained regions detected by bulk ATAC-seq (present in both asynchronous and synchronous cells) belonged to the unbookmarked regions of the scATAC-seq analysis (fig. S2F), highlighting the irreplaceability of scATAC-seq in analyzing mitotic bookmarking.

Next, we used GREAT (*33*) to investigate the potential biological functions of the bookmarked regions, and the associated genes were found to be enriched for housekeeping functions, including RNA transcription and processing (fig. S2G). This suggested that the bookmarked regions were functional elements for basic cellular processes rather than specific cell identity, which may be a common feature among other cell types. Thus, we performed the same analysis for bulk ATAC-seq data of HepG2 and HUH7 cells and found that 83% of the bookmarked regions were open in both datasets (fig. S2, H and I). Indeed, ~94% of the identified bookmarked regions were open in publicly accessible ATAC-seq datasets of 135 tissues/cell lines (Fig. 2C), confirming that the bookmarked regions were kept open across different cell types. In addition, genomic location distribution and chromatin state analysis showed that ~79% of the bookmarked regions were located in gene promoters and close to transcription start sites (TSSs), in sharp contrast to that of unbookmarked regions (fig. S2, J and K), further highlighting the maintenance of accessibility at promoters (*8*). Furthermore, we observed a significant overlap between the mitotically bookmarked regions and common Pol II binding sites from Pol II chromatin immunoprecipitation sequencing (ChIP-seq) datasets of 34 tissues/cell lines ($P < 0.0001$; Fig. 2D). These observations collectively suggest a relationship between the bookmarked regions and transcriptional potential.

Studies measuring nascent transcripts by 5-ethynyl uridine RNA sequencing (EU-RNA-seq) have revealed a hierarchical model of gene reactivation upon mitotic exit (*19*, *34*): Genes with basic cellular function, such as cellular organization, were first reactivated and defined as the first-wave genes, and cell type–specific genes were reactivated later and defined as the second-wave genes. To explore the functional composition and the hierarchical reactivation of the genes that are linked to the bookmarked regions, grouping analysis was performed according to the EU-RNA-seq dataset of human hepatoma cells, which contains information on the newly synthesized transcripts at 0, 40, 80, 105, 165, and 300 min after mitotic block release (*34*). The proportion of the first-wave genes associated with the bookmarked regions was higher than that of the second-wave genes and the genes related to the unbookmarked regions (Fig. 2E). In addition, gene reactivation of the bookmarked

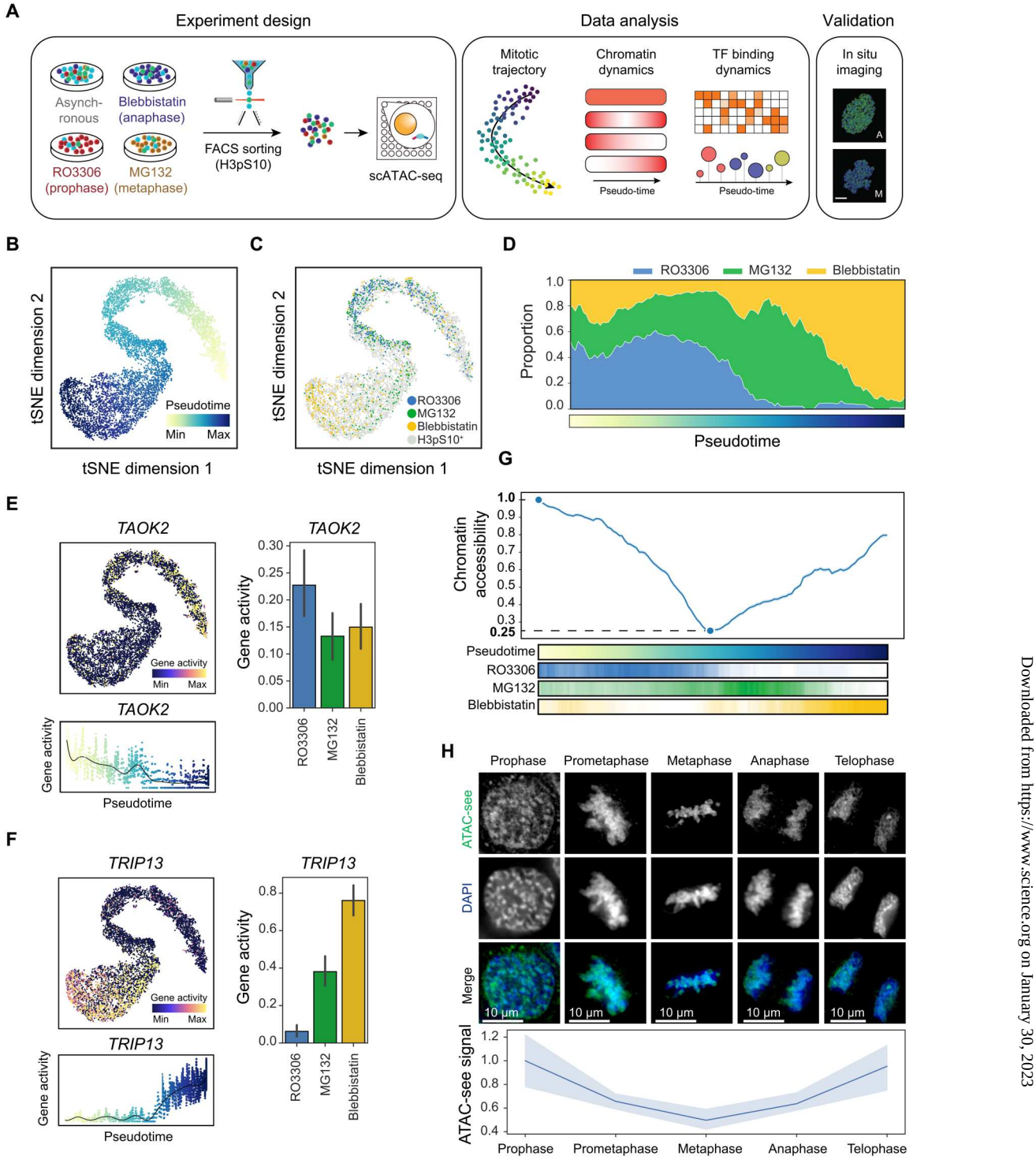

Fig. 1. Mitotic chromatin accessibility landscape established by scATAC-seq. (**A**) Schematic overview of the study design. (**B**) Inferenced pseudotime of 6538 mitotic L02 cells by Slingshot. The color bar indicated the pseudotime of each cell. (**C**) A tSNE projection of the 6538 mitotic L02 cells. Different colors represent unsynchronized or drug-treated H3pS10^{+} cells. (**D**) Proportion of drug-treated cells at 122 evenly sized time windows across the pseudotime trajectory. The color bar in the bottom indicated the pseudotime. (**E** and **F**) tSNE projections colored by the gene activity demonstrating the log-normalized chromatin accessibility around the loci of *TAOK2* (E) and *TRIP13* (F). The gene activity was calculated as the average normalized counts of all open regions located within ±20 kb of a gene's transcription start site (TSS). Bottom: Change in gene activity for the corresponding gene during pseudotime. Right: Gene activity of mean ± SD of cells in three drug-treated groups. (**G**) Overall chromatin accessibility across the pseudotime trajectory. (**H**) Representative immunofluorescence images of ATAC-see in mitotic L02 cells. Bottom: Quantification of the ATAC-see signal from L02 cells at five mitotic phases (n = 3 for each group). The ATAC-see raw signal was subtracted from the background intensities and then normalized against DAPI values to account for any variations in staining or image acquisition. Scale bars, 10 μm.

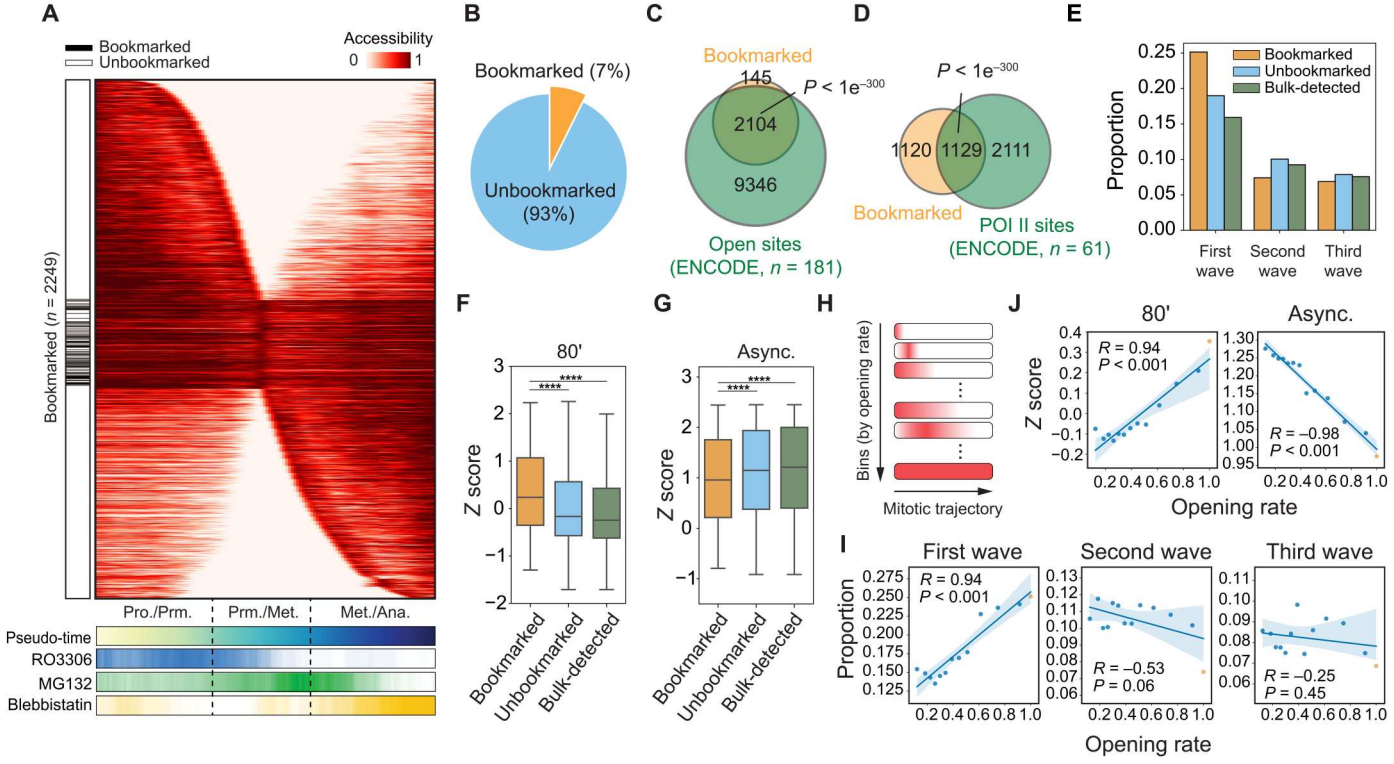

Fig. 2. Bookmarked regions that retained accessibility throughout mitosis were associated with rapid gene reactivation. (**A**) Chromatin accessibility dynamics of 30,671 open regions across the pseudotime trajectory. The black annotation indicated bookmarked regions open throughout the pseudotime trajectory. (**B**) Pie chart indicating the percentages of the bookmarked and unbookmarked regions in all open regions. (**C** and **D**) Venn diagram showing the overlap between the bookmarked regions and the open sites of 181 ATAC-seq datasets (C) or the common Pol II binding sites of 61 ChIP-seq datasets (D) collected from ENCODE. Statistical significance was determined by a chi-square test. (**E**) Percentage of the three transcriptional wave genes (*34*) in the genes near the bookmarked, unbookmarked, and bulk-detected regions. Genes near the open regions were annotated by HOMER. (**F** and **G**) *Z*-scaled expression of the reactivated genes (*34*) near the bookmarked, unbookmarked, and bulk-detected regions at 80 min after mitotic release (F) or in interphase (G). Statistical significance was determined by a two-sided Student's *t* test. ****$P < 0.0001$. (**H**) Schematic diagram for equally dividing the identified 30,671 open regions into 13 open chromatin bins according to the opening rate (see Materials and Methods). (**I** and **J**) Scatter plots showing the Pearson correlation between the opening rate of the open chromatin bin and the proportion (I) or expression (J) of the transcriptional wave genes (*34*) in the genes near the bin's open regions.

regions was significantly higher than that of the unbookmarked regions at 80 min after mitotic release when the first-wave genes started to be expressed (*34*), while the opposite was true in interphase cells ($P < 0.0001$; Fig. 2, F and G). These results suggested that the bookmarked regions were mainly related to the reactivation of the first-wave genes.

We also stratified all chromatin regions according to their opening rate (the proportion of sliding windows that are open across the mitotic trajectory; as such, the bookmarked regions were 100%) to examine the relationship between chromatin accessibility dynamics and transcription activation (Fig. 2H; see Materials and Methods). The opening rate of the chromatin regions was found to be positively correlated with the proportion of the associated first-wave genes ($R = 0.94$; Fig. 2I) and with the expression of reactivated genes at 80 min after mitotic release ($R = 0.94$; Fig. 2J). Similar correlations were observed when we repeated the analysis using another publicly accessible EU-RNA-seq dataset of human osteosarcoma cells (U2OS) (fig. S2, L to O) (*19*).

Together, these results suggest a functional potential for mitotic bookmarking: Bookmarked chromatin regions retained accessibility throughout mitosis for rapid reactivation of the associated genes (especially the first-wave genes) after mitosis.

The dynamic association of TFs with chromatin-accessible regions

As open chromatin is often occupied by TFs (*15*) and we have shown that chromatin accessibility begins to increase when chromosomes start to segregate, we investigated which TFs exert potential regulatory functions after metaphase. To explore how TFs dynamically interact with chromatin during mitosis, we first inferred the enrichment score for each TF in the JASPAR database based on hypergeometric test–based motif scanning (see Materials and Methods). Then, we calculated the Pearson correlation coefficient (ρ) between the enrichment score and pseudotime for each of the TFs, which yielded 110 mitotically lost TFs (i.e., $\rho < 0$) and 131 mitotically enriched TFs ($\rho > 0$) (Fig. 3A and fig. S3A). Specifically, the enrichment score of mitotically lost TFs [e.g., CTCF, PAX5, and ASCL1, all of which are known to dissociate from mitotic chromosomes (*35*, *36*)] was reduced as mitosis progressed. The mitotically enriched TFs, on the other hand, contained some known bookmarking TFs, such as RUNX2 (*13*) and MYC (*37*), and highly overlapped with TFs enriched on mitotic chromosomes observed in living cells (fig. S3B) (*9*). The elevated enrichment score of these mitotically enriched TFs as mitosis progressed suggested that they may play a regulatory role after metaphase (Fig. 3A and fig. S3A).

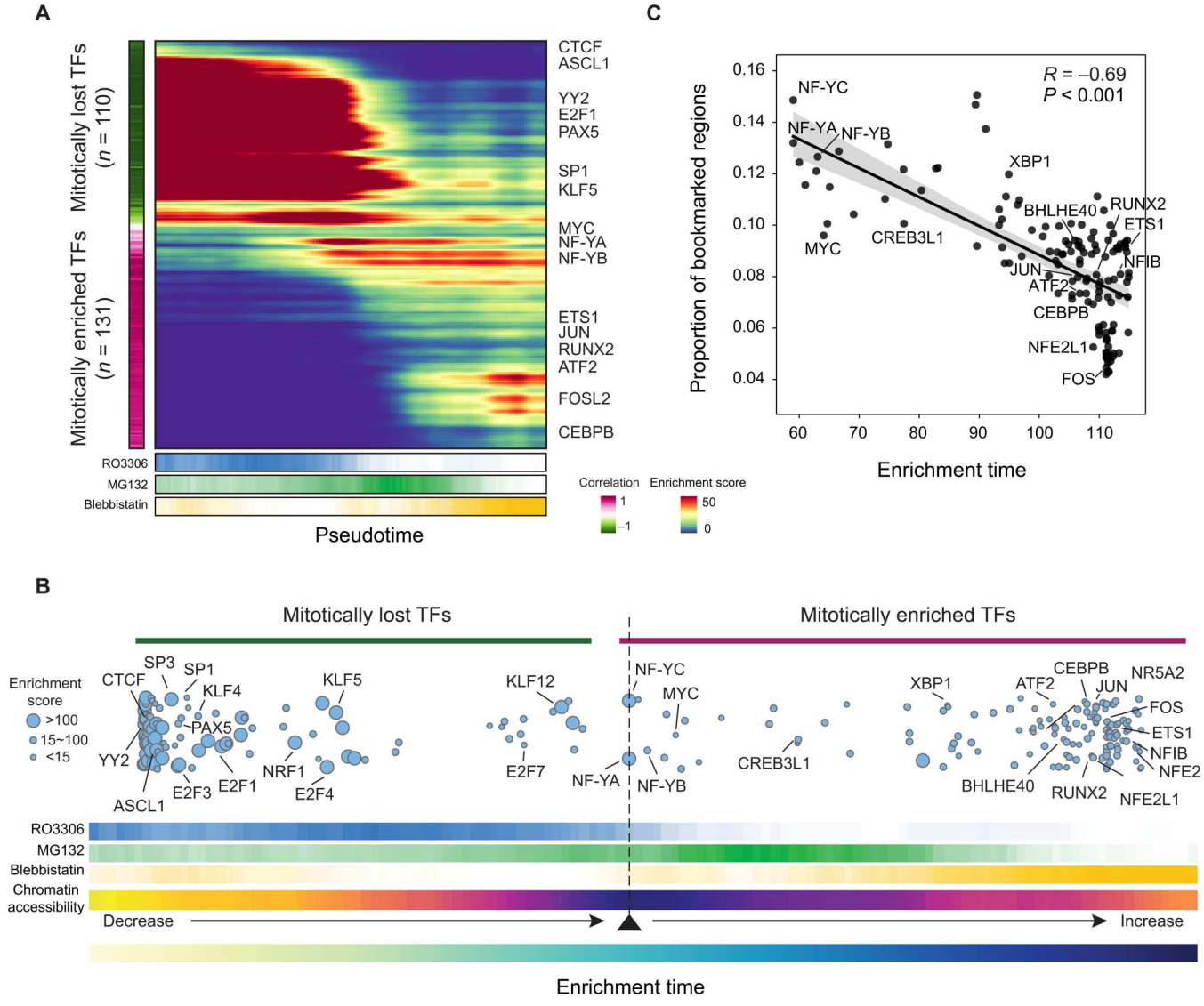

Fig. 3. Dynamics of transcription factor enrichment during mitosis. (**A**) Heatmap showing the enrichment score of the 241 TFs along the pseudotime trajectory. The color bar to the left of the heatmap indicated the Pearson correlation coefficient (ρ) between TF's enrichment score and pseudotime. (**B**) Bubble plots showing the dynamics of TF occupancy to chromatin along the pseudotime trajectory. The position of each bubble along the *x* axis indicated the pseudotime at which the TF reached its maximum enrichment score, which was defined as the TF's enrichment time. The size of the bubble represented the average enrichment score of that TF in the pseudotime trajectory. The color bar in the bottom indicated the proportion of each drug-treated group in the window, chromatin accessibility, and enrichment time along the trajectory. (**C**) Scatter plot showing the Pearson correlation between TF enrichment time and the proportion of bookmarked regions in TF-targeted regions. Each dot represented a mitotically enriched TF, and the TF-targeted regions were defined as the open regions containing the TF motif.

To clearly present the dynamic association/dissociation of the TFs, we plotted each TF based on the pseudotime when it reached the maximum enrichment score, which we termed the TF's "enrichment time" (Fig. 3B). As expected, enrichment of mitotically enriched TFs occurred along with an increase in chromatin accessibility (fig. S3C). Consistently, in the EU-RNA-seq dataset of HUH7, we found that the enrichment time of mitotically enriched TFs from the first wave was significantly earlier than that from the second wave ($P < 0.001$; fig. S3, D to G), confirming that the TFs work in a temporal order in gene reactivation. In particular, the enrichment time of some early-enriched TFs from the first wave, such as NF-YA, NF-YB, and ZNF449, matched with metaphase, and their enrichment score decreased as mitosis progressed to anaphase. The expression of these TFs peaked at 80 min and then decreased (fig. S3, D to F). These results suggested that the early-enriched TFs were likely to play a regulatory role early upon mitotic exit.

For a given mitotically enriched TF, we identified candidate targeted regions as those containing predicted binding motifs for that specific TF. We found that the enrichment time was negatively correlated with the proportion of targeted bookmarked regions ($R = -0.69$; Fig. 3C and fig. S3H). This indicated that early-enriched TFs, such as MYC, which is known for promoter binding, were more likely to occupy bookmarked regions. Notably, we observed that NF-Y subunits (NF-YA and NF-YB) were enriched earlier

than other mitotically enriched TFs and targeted a high proportion of bookmarked regions (13%). Considering the rapid expression of NF-Y subunits during mitotic exit (fig. S3, E and F), our finding suggested that NF-Y is a candidate bookmarking TF to promote rapid gene reactivation.

In addition, we found that late-enriched TFs contained some TFs mainly occupying distal enhancers (Fig. 3B and fig. S3I), such as CEBPB (*38*) and JUN (*39*), which are known to be key regulators during liver regeneration. Since enhancers are related to cellular identity (*7*), these results suggested a hierarchical TF binding map during postmetaphase genome decondensation, in which open chromatin was first occupied by promoter-bound TFs, followed by TFs that targeted more distal enhancers, which mirrored the hierarchical pattern of postmitotic gene reactivation (*34*).

NF-YA is a bookmarking TF that preferentially occupies bookmarked regions

To search for the key bookmarking TFs, we performed TF binding motif enrichment analysis on the bookmarked regions. We found that the known NF-YA motif CCAAT is the most enriched motif in these regions (Fig. 4A). NF-YA is the sequence-specific DNA binding subunit of the NF-Y complex (*40*), and its locus is highly accessible throughout mitosis (fig. S4A). Immunofluorescence staining (*41*) of NF-YA confirmed its chromatin binding throughout mitosis in L02 cells (Fig. 4B).

Our previous motif prediction analysis showed that NF-YA may play a regulatory role early in mitotic exit by binding to bookmarked regions (Fig. 3, B and C, and fig. S3F). To determine the genomic occupancy of NF-YA in mitosis, we performed cleavage under targets and tagging (CUT&Tag) experiments on mitotic L02 cells (see Materials and Methods). A total of 5,088 NF-YA binding sites were detected by CUT&Tag analysis, one of which was located in the promoter of the known target gene *HLA-DRA* (fig. S4B) (*42*). We found that 86% of NF-YA binding sites included the NF-YA motif (fig. S4C), indicating that NF-YA binds to mitotic chromatin in a sequence-specific manner.

Seventy-nine percent of NF-YA binding sites overlapped with mitotic open regions (fig. S4D). For the open regions occupied by NF-YA, we found that the binding signal of NF-YA from CUT&Tag analysis was significantly positively correlated with their accessibility from scATAC-seq ($R = 0.70$, $P < 0.001$; Fig. 4C and fig. S4E). Importantly, ~61% of the bookmarked regions were found to be occupied by NF-YA (Fig. 4D), establishing a strong association of NF-YA binding with mitotic bookmarking. Moreover, NF-YA binding was enriched at the TSS of the postmitotic reactivated genes, especially those of the first-wave genes (Fig. 4E), such as *PDZD8*, *MPC1*, and *ACAA1* (Fig. 4F). In contrast, the promoters of late-reactivating genes, such as *POLE2*, *PBK*, and *FANCD2*, do not harbor the NF-YA binding site (fig. S4F). Consistently, the expression of reactivated genes targeted by NF-YA was significantly higher 80 min after mitotic release than those not occupied by NF-YA ($P < 0.0001$; Fig. 4G).

A very recent study proposed that rapid gene reactivation is most accurately predicted by a combination of retained chromatin accessibility, histone modification of H3K27ac, and TF TBP binding (*6*). Following their method, we investigated the relationship between the binding of NF-YA and the retention of seven bookmarking factors by analyzing published ChIP-seq datasets (see Materials and Methods). We found that the NF-YA binding sites had a significant overlap with the bookmarked regions, the retained H3K27ac-modified regions, and the retained TBP binding sites ($P < 0.0001$; fig. S4G) (*6*). More than 50% of the NF-YA binding sites overlapped with the peaks of at least one of the abovementioned three bookmarking factors (fig. S4H). Collectively, these results suggest that NF-YA is a bookmarking TF that preferentially occupies bookmarked regions and may contribute to rapid gene reactivation after mitosis.

The NF-Y complex is composed of the NF-YA subunit and NF-YB/NF-YC dimer (*40*). Motif analysis and coimmunoprecipitation assays together indicated that NF-YA and NF-YB interact during mitosis (fig. S4, I and J). To explore whether NF-YA and NF-YB occupy the similar bookmarked regions, we performed NF-YB CUT&Tag analysis on mitotic L02 cells. We found that the genome-wide binding profile of NF-YA and NF-YB was significantly correlated in terms of genomic position and binding signal intensity ($R = 0.72$, $P < 0.001$; fig. S4, K and L). More than 80% of the bookmarked regions occupied by NF-YA or NF-YB were NF-YA and NF-YB co-binding regions (fig. S4M). These results collectively suggest that NF-YA and NF-YB can contact each other as a complex to occupy the bookmarked regions during mitosis.

NF-YA KD impaired postmitotic transcriptional reactivation

To further explore the biological function of NF-YA in mitotic exit, we next knocked down NF-YA by transfecting L02 cells with two independent short hairpin RNAs (shRNAs) and assessed the impacts on postmitotic transcriptional reactivation (fig. S5A; see Materials and Methods). Consistent with a previous report (*43*), NF-YA KD significantly reduced DNA synthesis, corroborating NF-Y's established role in proliferation ($P < 0.05$; fig. S5, B and C). We performed ATAC-see on control and NF-YA KD cells and observed that NF-YA KD cells had reduced overall chromatin accessibility in telophase (Fig. 5, A and B), suggesting the potential role of NF-YA in chromatin accessibility expansion, in addition to its bookmarking function. We also pulsed L02 cells with EU to label nascent RNAs, which were evident in the telophase of the control cells, while the overall signal intensity was significantly reduced in the NF-YA KD cells ($P < 0.001$; Fig. 5, C and D, and fig. S5, D and E), indicating that NF-YA KD impaired postmitotic transcriptional reactivation.

To illustrate the reactivation of genes affected by NF-YA KD, we used RNA-seq (*44*) to profile global gene expression in control and NF-YA KD cells upon mitotic exit. Compared with control cells, we identified 2673 differentially expressed genes in NF-YA KD cells, of which 540 were up-regulated and 2133 were down-regulated (Fig. 5E and fig. S5F). Specifically, genes with known functions in chromatin remodeling (*SMARCA1* and *SMARCD3*) and RNA transcription (*KAT2B*, *DHX33*, and *NCBP2*) were down-regulated in NF-YA KD cells (Fig. 5F). Furthermore, we found that the expression of the first-wave genes was decreased overall after NF-YA KD (Fig. 5G), indicating the importance of NF-YA in the reconstruction of basic cellular function after mitosis. In addition, we found that the second-wave and third-wave genes were also globally down-regulated in NF-YA KD cells (Fig. 5G). This result was supported by the decreased expression of multiple genes reported to be involved in liver development (*PROX1*, *JUN*, *ONECUT2*, *GATA4*, and *GATA6*), DNA replication, and G_1-S transition (*NF-YA*, *CUX1*, and *CCNE1*) after NF-YA KD (fig. S5, G and H).

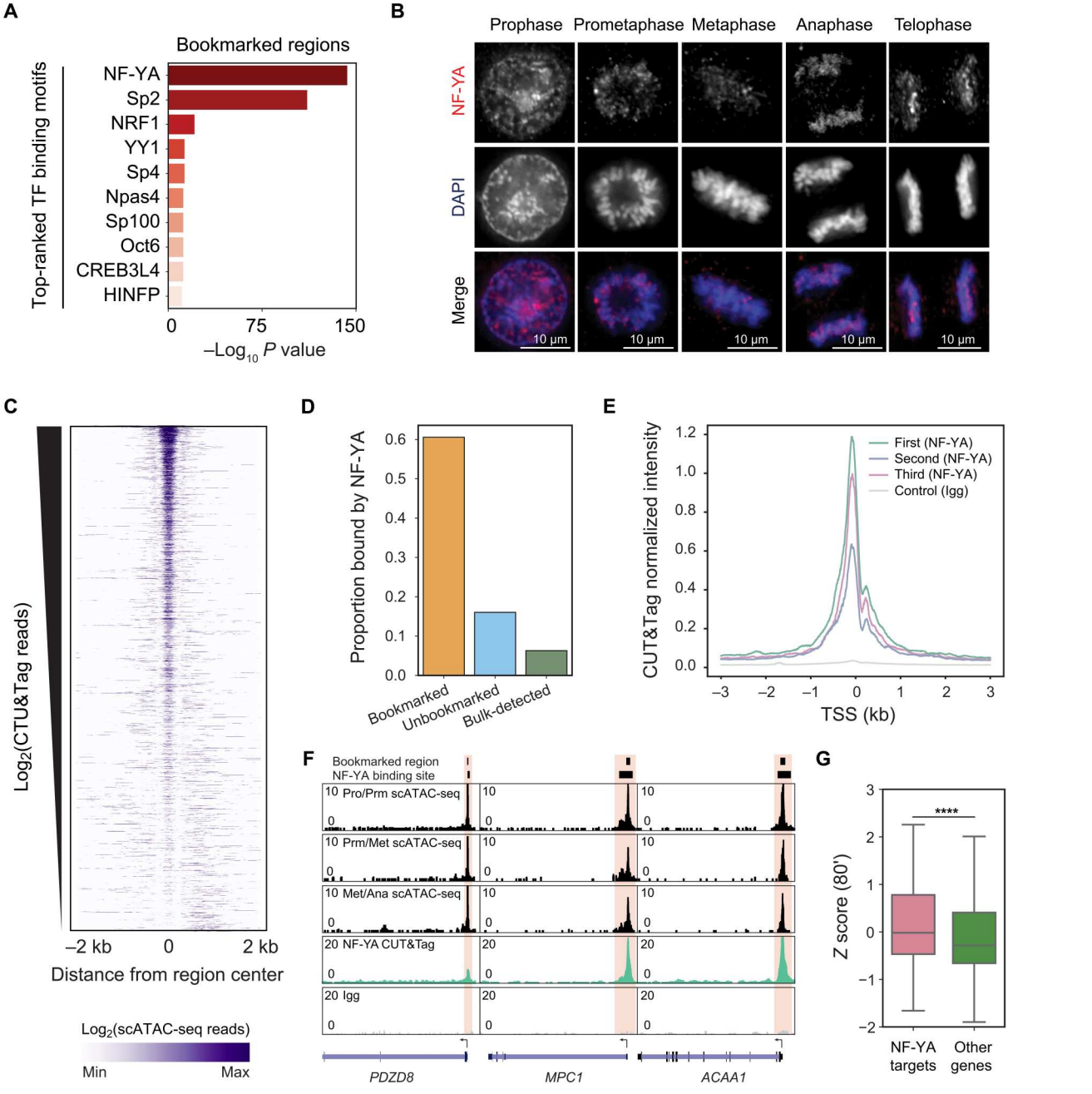

Fig. 4. NF-YA preferentially occupies bookmarked chromatin regions for transcriptional reactivation. (**A**) Top enriched TF binding motifs in the bookmarked regions. (**B**) Representative immunofluorescence images of NF-YA localization in mitotic L02 cells. Cells were labeled with NF-YA (red) and DAPI (blue). Scale bars, 10 μm. (**C**) Heatmap of chromatin accessibility around the center of NF-YA–bound open regions, ordered by NF-YA CUT&Tag read counts. (**D**) Proportion of regions in the bookmarked, unbookmarked, and bulk-detected regions occupied by NF-YA from CUT&Tag analysis. (**E**) CUT&Tag normalized intensity around the TSSs of three transcriptional wave gene sets in the EU-RNA-seq dataset of Palozola *et al*. (*34*). For a given gene set, the CUT&Tag normalized intensity was defined as the average count of all genes in the gene set. (**F**) Normalized UCSC genome browser tracks of chromatin accessibility from scATAC-seq and NF-YA occupancy from CUT&Tag profiling in the *PDZD8*, *MPC1*, and *ACAA1* loci. The orange shading highlights the bookmarked regions that were occupied by NF-YA. (**G**) *Z*-scaled expression of NF-YA targeted and other reactivated genes at 80 min after mitotic release in the EU-RNA-seq dataset of Palozola *et al*. (*34*). Statistical significance was determined by a two-sided Student's *t* test. ****$P < 0.0001$.

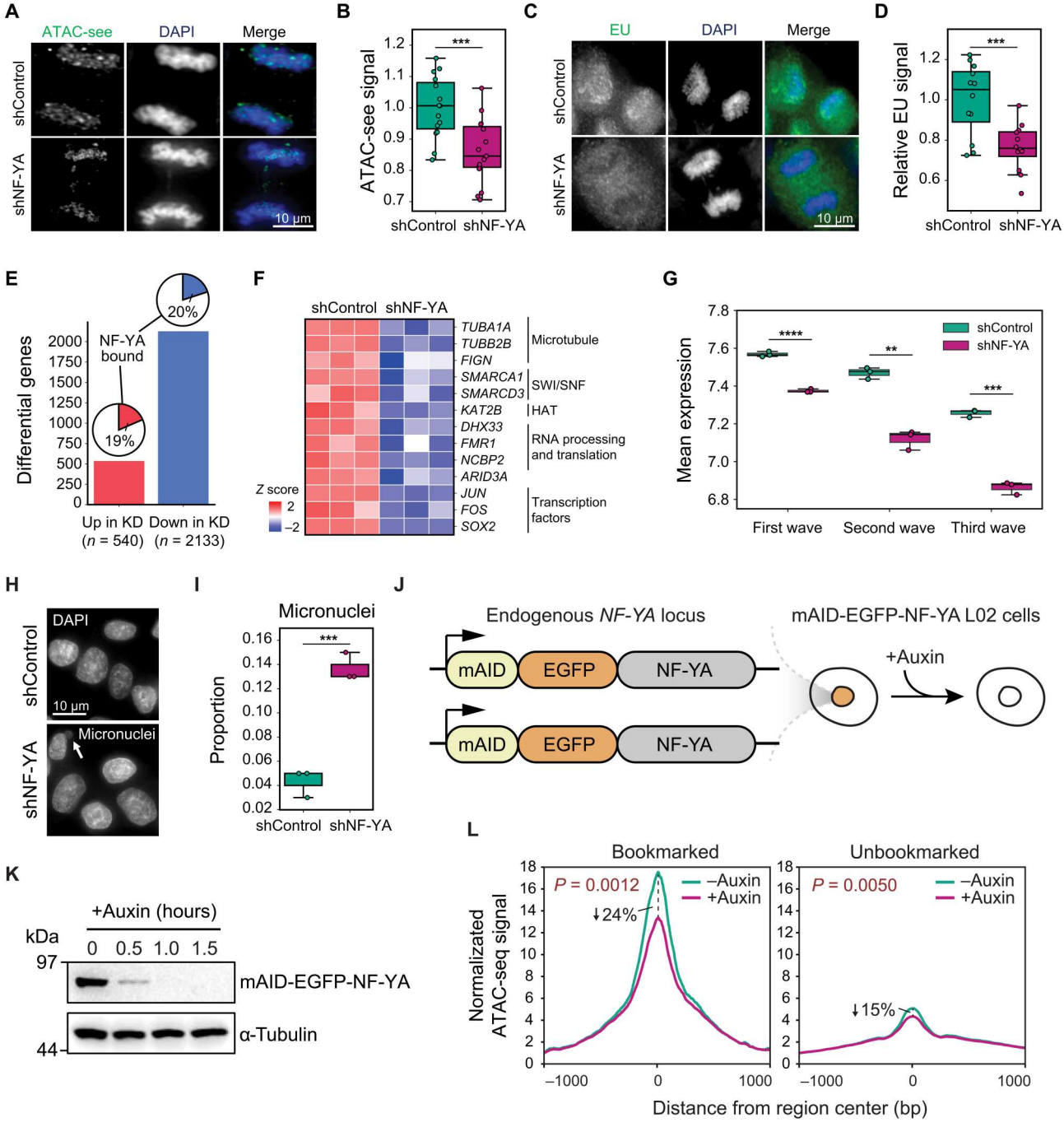

Fig. 5. Loss of NF-YA activity impairs postmitotic transcriptional reactivation. (**A**) Representative immunofluorescence images of ATAC-see (green) in shControl and shNF-YA L02 cells counterstained with DAPI (blue). Scale bar, 10 μm. (**B**) Statistical analyses of the ATAC-see signal in (A) by a two-sided Student's *t* test. ***$P < 0.001$. (**C**) Representative immunofluorescence images of EU (green) in shControl and shNF-YA L02 cells. L02 cells were labeled with EU (green) and DAPI (blue). Scale bar, 10 μm. (**D**) Statistical analyses of the EU signal in (C) by a two-sided Student's *t* test. ***$P < 0.001$. (**E**) Differential expression analysis between the control and NF-YA KD cells. The pie chart showed the proportion of differentially expressed genes bound by NF-YA. (**F**) Heatmap showing the *z*-scaled gene expression of specific differentially expressed genes in control and NF-YA KD cells. (**G**) Mean expression of three transcriptional wave genes (*34*) in control and NF-YA KD cells. Statistical significance was determined by a two-sided Student's *t* test. **$P < 0.01$; ***$P < 0.001$; ****$P < 0.0001$. (**H**) Representative immunofluorescence images of nuclei in shControl and shNF-YA L02 cells. The white arrow indicated the cells with micronuclei. Scale bar, 10 μm. (**I**) Statistical analyses of interphase cells with micronuclei in (H) by a two-sided Student's *t* test. ***$P < 0.001$. (**J**) Schematic diagram showing the construction of L02 mAID-EGFP-NF-YA cell line and auxin-inducible degradation of the tagged NF-YA. (**K**) Degradation of mAID-EGFP-NF-YA was evaluated by Western blot. (**L**) ATAC-seq signal in untreated (−auxin) and auxin-treated (+auxin) mitotic L02 cells on bookmarked or unbookmarked regions. Statistical significance was determined by a two-sided Wilcoxon rank-sum test.

We also found that genes involved in DNA damage repair (*PARP1*, *MDM2*, *STK11*, and *USP11*), telomere maintenance (*TERT*), and centrosome duplication (*SUFU*) were down-regulated after NF-YA KD (fig. S6A), all of which have been reported to play a role in maintaining genomic stability. The overall expression of genes associated with genomic stability was also decreased in NF-YA KD cells (fig. S6, B and C). Notably, we observed micronuclei, one of the hallmarks of genomic instability and generally due to chromosomal segregation defects (*45*), in ~13% of the NF-YA KD cells, which was ~3 times more frequent than in the control cells (Fig. 5, H and I). To confirm this, we conducted a time-lapse imaging experiment to examine mitotic progression (see Materials and Methods). Compared to the control cells, ~12% of the NF-YA KD cells had a nucleoplasmic bridge that could result in micronucleus formation, while this ratio was only ~4% in control cells (fig. S6, D and E). Since the transcriptional activity of chromosomes/chromatids (fragments) in the micronucleus may be missing (*46*), our findings suggest that NF-YA bookmarking established competence for proper gene reactivation upon mitotic exit.

To further confirm the bookmarking role of NF-YA during mitosis, we depleted the NF-YA protein by using a mini-auxin–inducible degron (mAID) system (*47*) that enables acute degradation of NF-YA protein over a short period of time (see Materials and Methods). Specifically, we engineered L02 cell line in which N termini of both *NF-YA* alleles were fused to the mAID-EGFP (enhanced green fluorescent protein) elements (Fig. 5J and fig. S7A). Western blot analysis showed that upon 1-hour treatment with auxin, NF-YA expression was substantially reduced (Fig. 5K). We applied auxin to specifically deplete NF-YA in mitotic cells, followed by EU labeling. We found that the overall EU signal intensity was significantly reduced in NF-YA–depleted telophase cells compared to control telophase cells ($P < 0.0001$; fig. S7, B to E). Loss of NF-YA during mitosis also resulted in increased frequency of micronuclei in cells (fig. S7, F and G). These results were consistent with the phenotypic outcome by shRNA KD, further highlighting the bookmarking role of NF-YA in postmitotic gene reactivation.

Given the potential association of NF-YA binding with chromatin accessibility (Fig. 4C and fig. S4E), we next asked whether NF-YA is necessary for maintaining open chromatin during mitosis. We used the AID system to acutely deplete NF-YA in mitosis and then performed ATAC-seq analysis on control and NF-YA–depleted mitotic cells (fig. S7H). We found that upon NF-YA loss, the chromatin accessibility of the mitotic open regions was significantly reduced, especially in the bookmarked regions ($P < 0.01$; Fig. 5L), suggesting that NF-YA retention at the bookmarked regions during mitosis may contribute to the maintenance of accessible chromatin organization.

DISCUSSION

Mitotic bookmarking is essential for the proper reestablishment of transcriptional programs after cell division (*48*). Using scATAC-seq technology, we analyzed thousands of mitotic cells at variable stages and generated the landscape of chromatin accessibility and its dynamics during mitosis at single-cell resolution (fig. S8). Our analysis shows that most mitotic chromatin regions underwent dynamic closing and reopening, but only a subset of the chromatin regions retained accessibility throughout mitosis as bookmarks, whose signals were often "diluted" beyond detection in bulk cell analysis. These bookmarked chromatin regions are preferentially occupied by NF-YA, which regulates the reactivation of genes after mitotic exit. We also provided experimental support for the bookmarking function of NF-YA in postmitotic gene reactivation.

Our findings provide two insights into the underlying mechanism of the hierarchical model of gene reactivation after mitosis (*19*, *34*). On the one hand, the bookmarked regions were generally at the promoters of the rapidly reactivated housekeeping genes. Promoter accessibility strongly correlates with gene expression, suggesting that bookmarked regions may ensure rapid reactivation of these genes after mitosis. On the other hand, by tracking the genome-wide binding dynamics of the 131 mitotically enriched TFs, a rapid enrichment of promoter-bound TFs compared with a slower occupancy of enhancer-bound (usually cell type–specific) TFs was observed. This temporal order of TF association also reflects the hierarchical model of gene reactivation (*19*, *34*), suggesting that the order in which transcriptional programs are rebuilt may depend on the dynamic pattern of gene regulation after metaphase.

The bookmarked regions seem to be relatively conserved across multiple cell types; in contrast, cell-specific chromatin accessibility is highly dynamic during mitotic progression. This may explain why some cell-specific TFs have been found to dynamically interact with mitotic chromatin (*10*, *11*). An impressive phenomenon is that the mitotic nuclei of somatic cells are more likely to be reprogrammed with the support of fertilized mitotic oocytes than interphase nuclei (*49*, *50*). Thus, the high dynamics of cell-specific chromatin accessibility make mitosis a short window of opportunity to reshape transcriptional programs and promote changes in cell fate.

Mitotic bookmarking by TF binding facilitates the postmitotic reestablishment of transcriptional programs (*36*). However, the exploration of potential bookmarking TFs is mostly based on the mitotic binding test for some specific TFs (*10*, *12*, *14*), which limits the de novo discovery of bookmarking TFs. By performing TF binding motif enrichment analysis and integrating CUT&Tag data, we proposed that NF-YA is a bookmarking TF that preferentially occupies the bookmarked regions. We validated the bookmarking function of NF-YA by showing that NF-YA KD impaired the reactivation of thousands of genes, including some transcription-related genes. Mitotic binding of NF-YA is also detected in other cell types (*42*), suggesting a universal bookmarking function of NF-YA.

Since loss of NF-YA during mitosis impairs chromatin accessibility, maintenance of the bookmarked regions may require the presence of NF-YA. This idea is supported by previous observations that NF-Y is essential for maintaining accessible chromatin in many contexts (*51*–*53*). For example, NF-YA's unique DNA binding mode, which induces an ~80° bend in the DNA through insertion of the NF-YA A2 helix into the DNA minor groove (*40*), may promote binding of other TFs by making their recognition sequences more accessible (*52*, *53*). In addition, NF-YA can function as an NF-Y complex by contacting the NF-YB/NF-YC dimer during mitosis. The histone-fold domain of the NF-YB/NF-YC dimer enables NF-Y to displace nucleosomes (*40*), placing NF-Y–bound chromatin in a nucleosome-depleted state (*53*). Thus, it is tempting to speculate that the sequence-specific targeting capability of NF-Y (by the NF-YA subunit), along with nucleosome-like properties (by the NF-YB/NF-YC dimer) (*52*), allows NF-Y to stably occupy bookmarked regions and maintain their accessibility during mitosis.

Approximately 80% of the genes affected by NF-YA KD are not directly targeted by NF-YA, suggesting that NF-YA has multiple ways to promote postmitotic transcriptional activation. One possible way is that NF-YA promotes postmitotic chromatin remodeling because NF-YA KD affects the expansion of chromatin accessibility and the expression of genes with chromatin remodeling functions. In addition, by interrogating CUT&Tag data, we observed that NF-YA targeted some mitotically enriched TFs, suggesting that NF-YA may function in the TF regulatory network to expand its regulatory range. Future 3D genomics in combination with super-resolution imaging technologies (*41*, *54*) will help elucidate the multiple roles of NF-YA in postmitotic transcriptional activation.

In summary, our findings delineate a dynamic and regulatory map of mitotic chromatin accessibility that reveals important bookmarking factors and provides insights into the molecular mechanism that promotes hierarchical transcriptional reactivation.

MATERIALS AND METHODS

Cell culture and synchronization

The L02 cell line was a gift from C. Li of Nanjing University. The HepG2 cell line was purchased from the American Type Culture Collection (ATCC). The HUH7 cell line was purchased from CellBio. L02 cells, HepG2 cells, and HUH7 cells were cultured in Dulbecco′s modified Eagle′s medium (DMEM) (Invitrogen) supplemented with 10% (v/v) fetal bovine serum (FBS) (HyClone) and penicillin/streptomycin (100 U/ml and 100 μg/ml, respectively; Invitrogen) at 37°C in a humidified atmosphere with 8% CO_2. To enrich prophase cells, cells were blocked with 9 μM RO3306 for 20 hours. To enrich metaphase cells, cells were first blocked with 2.5 mM thymidine for 24 hours followed by a release in fresh culture medium for 9 hours. Then, the cells were exposed to 20 μM MG132 for another 2 hours. To enrich anaphase cells, cells were first blocked with 2.5 mM thymidine for 24 hours and subsequently released in fresh culture medium for 9 hours. Then, the cells were exposed to 50 μM blebbistatin for another 2 hours. For some indicated experiments, prometaphase cells were enriched by nocodazole (100 ng/ml) for 16 hours and collected by mitotic shake-off.

Antibodies and chemical inhibitors

Anti–NF-YA antibody (mouse, sc-17753; Santa Cruz Biotechnology) and anti-H3pS10 antibody (rabbit, 53348; Cell Signaling Technology) were used for immunofluorescence. Anti–α-tubulin antibody (mouse; T9026, Sigma-Aldrich), anti-GFP antibody (rabbit, 2037; Cell Signaling Technology), anti–c-myc antibody (mouse, 67441-1; Proteintech), and anti–NF-YB antibody (mouse, sc-376546; Santa Cruz Biotechnology) were used for Western blotting. Anti–NF-YB antibody (rabbit; PA5-31913, Thermo Fisher Scientific) was used for NF-YB CUT&Tag. Draq7 (Ab109202; Abcam) and 4′,6-diamidino-2-phenylindole (DAPI) (28718-90-3, Sigma-Aldrich) were used to stain DNA. The appropriate secondary antibodies were purchased from Jackson ImmunoResearch Laboratories.

Nocodazole (100 ng/ml), RO3306 (9 μM), MG132 (20 μM), and blebbistatin (50 μM) were purchased from Sigma-Aldrich. Disuccinimidyl glutarate (DSG; 2 mM) was purchased from Thermo Fisher Scientific. EU (2 mM) was purchased from Invitrogen.

Immunofluorescence

A detailed protocol for immunofluorescence is well documented, as previously described (*41*). Briefly, L02 cells growing on coverslips after drug treatment were prefixed with DSG for 50 min at room temperature (RT), followed by 15-min fixation with 1% formaldehyde (FA). The fixed cells were then extracted with 0.1% Triton X-100 in phosphate-buffered saline (PBS) for 10 min. After being washed three times with PBST (0.05% Tween 20 in PBS), the cells were blocked with 1% bovine serum albumin (BSA; Sigma-Aldrich) in PBST for 1 hour and then incubated with primary antibodies for 2 hours and secondary antibodies for 1 hour at RT. DNA was stained with DAPI (Sigma-Aldrich). Images of 2D cell culture were acquired every 0.25 μm at the *z* axis to generate 3D image stacks using an Olympus 60×/1.42 Plan APO N objective on an Olympus IX71 microscope (Applied Precision DeltaVision). The 3D image stacks were deconvolved and projected with SoftWoRx (Applied Precision) and mounted in figures with Photoshop and Illustrator (Adobe). Fluorescence was quantified with ImageJ software (National Institutes of Health) and Illustrator (Adobe).

Immunoprecipitation

Mitotic L02 cells were collected and lysed in immunoprecipitation (IP) buffer [50 mM Hepes (pH 7.4), 150 mM NaCl, 2 mM $MgCl_2$, 1 mM EGTA, 0.1% Triton X-100, and 1 mM dithiothreitol] supplemented with protease inhibitor cocktail. Cell lysates were clarified by centrifugation at 12,000 rpm for 20 min at 4°C. Clarified cell lysates were incubated with NF-YA antibody–conjugated protein A/G resin or immunoglobulin G (IgG)–conjugated protein A/G resin for 4 hours at 4°C. The binding fraction was washed with IP buffer three times before being resolved by SDS–polyacrylamide gel electrophoresis and immunoblotted with the indicated antibodies.

Cell line generation

To generate L02 cells endogenously expressing mAID-EGFP-NF-YA, we took advantage of the CRISPR-Cas9–based knock-in method to place the mAID sequence and EGFP sequence at the N terminus of the *NF-YA* gene. *NF-YA*–targeting single-guide RNA (sgRNA) was cloned by annealing oligos CACCgtttgctgtatactgctcca and AAACtggagcagtatacagcaaac into the plasmid containing Cas9 to introduce a double break at the targeted genomic location of NF-YA. The donor plasmid contains a short homology arm with the following primers: caatatgaccgccatgttatggccacaagtcctcttgc and aactgacacacattccacggccctttgtggaatcccttcc and therefore can be inserted into the targeted genomic location of NF-YA. To generate cell lines expressing endogenously tagged NF-YA, L02 cells were transfected with the sgRNA expression plasmid and the donor plasmid for NF-YA at a ratio of 1:1 (micrograms). Twenty-four hours after the transfection, puromycin (5 μg/ml) was added to select the positive transfected cells for another 72 hours. Individual colonies were picked, and single clones were isolated by limited dilution. Homozygous gene-edited clones were identified by immunoblotting with NF-YA antibody. To induce rapid degradation of NF-YA, the human codon–optimized E3 ubiquitin ligase from OsTIR1 was stably introduced into mAID-EGFP-NF-YA cells using lentiviral system. After 48 hours of transfection, blasticidin (5 μg/ml) was added for 2 weeks. Individual colonies were picked, and single clones were isolated by limited dilution and verified by immunofluorescence analysis and Western blotting with GFP antibody.

Tn5 transposome assembly

The assembly of the Tn5 transposome was performed according to a previously described method (*31*) with modifications. Briefly, each oligonucleotide (oligo) [Tn5ME-A-FITC (fluorescein isothiocyanate), Tn5ME-B-FITC, and Tn5MErev] was resuspended in water to a final concentration of 100 μM. Then, equimolar amounts of Tn5MErev and Tn5ME-A-FITC, or Tn5MErev and Tn5ME-B-FITC, were mixed in separate polymerase chain reaction (PCR) tubes and denatured on a thermocycler at 95°C for 5 min followed by a slow cooling down on the thermocycler with power off. The Tn5 transposome was assembled into a 20-μl reaction system with the following components: 2 μl of Tn5MErev/Tn5ME-A-FITC, 2 μl of Tn5MErev/Tn5ME-B-FITC, 10 μl of glycerol (100% solution), 2 μl of 10× tris-buffered saline (TBS) buffer, and 4 μl of Tn5 transposome. The reagents were mixed thoroughly but gently, and the solution was left on bench at RT for 1 hour to allow annealing of oligos to Tn5.

ATAC-see

A detailed protocol for ATAC-see is well documented, as previously described (*31*). Briefly, the DSG- and 1% FA–fixed cells were permeabilized with lysis buffer [10 mM tris-HCl (pH 7.4), 10 mM NaCl, 3 mM $MgCl_2$, and 0.01% NP-40] for 10 min at RT. Then, the slides were rinsed with PBS three times and incubated with the transposase mixture solution [25 μl of 2× TD buffer, 100 nM Tn5-FITC, and add double-distilled water (ddH_2O) up to 50 μl] in a humid chamber box for 30 min at 37°C. After the transposase reaction, the slides were washed three times with PBS containing 0.01% SDS and 50 mM EDTA for 15 min each at 55°C. Last, the slides were mounted and imaged with Deconvolution microscope. For statistics, the ATAC-see signal was measured with ImageJ software. Briefly, the ATAC-see raw signal was subtracted from the background intensities and then normalized against DAPI values to account for any variations in staining or image acquisition.

CUT&Tag

The CUT&Tag assay was performed in strict accordance with the Hyperactive In Situ ChIp Library Kit from Illumina. After three washes with 1.5 ml of wash buffer, aliquots of mitotic L02 cells (60 to 100,000 cells) were incubated with 10 μl of activated concanavalin A–coated magnetic beads at RT for 10 min. Then, the bead-bound cells were pelleted and resuspended in 50 μl of DIG Wash buffer containing 2 mM EDTA and a 1:100 diluted primary antibody for another rotating incubation for 2 hours at RT. To increase the number of protein A binding sites for each bound primary antibody, an additional incubation with 1:100 diluted and species-matched secondary antibody (e.g., guinea pig anti-rabbit IgG antibody for a rabbit primary antibody) was performed in 50 μl of DIG Wash buffer at RT for 60 min. After the incubation, the bead-bound cells were washed in 800 μl of DIG Wash buffer for 5 min to remove unbound antibodies. Then, a 1:200 dilution of the pA-Tn5 adapter complex (~0.04 μM) was prepared in Dig-300 buffer, and 100 μl of the diluted adapter was added to the cells with gentle vortexing, followed by incubation at RT for 1 hour. Next, the cells were washed three times, 5 min each, in 800 μl of Dig-300 buffer to remove unbound pA-Tn5 protein, followed by resuspension in 300 μl of Tagmentation buffer (10 mM $MgCl_2$ in Dig-300 buffer) and incubation at 37°C for 1 hour. To stop tagmentation, 10 μl of 0.5 M EDTA, 3 μl of 10% SDS, and 2.5 μl of proteinase K (20 mg/ml) were added to the cells and incubated at 50°C for 60 min or overnight at 37°C. To extract the DNA, 150 μl of tris-phenol and 150 μl of chloroform were added to each tube followed by vortexing, quick spinning, and resting on bench for 5 min. Then, the tubes were placed on a magnet stand to pellet the beads, and the supernatant was carefully removed. Without disturbing the beads, the pellet was washed twice with 750 μl of 100% ethanol and air-dried for ~5 min; 25 to 30 μl of 1× Tris-EDTA (TE) were added, and the tubes were vortexed, quickly spun, and sat on bench for 5 min. To amplify the libraries, 24 μl of DNA was mixed with 5 μl of universal i5 and a uniquely barcoded i7 primer33 with different barcodes for each sample. After the addition of 10 μl of 5× TruePrep Amplify Buffer (TAB) buffer, the samples were placed in a thermocycler to run the following cycling conditions: 72°C for 3 min (gap filling); 98°C for 30 s; 14 cycles of 98°C for 15 s and 60°C for 30 s; final extension at 72°C for 30 s and hold at 4°C. Post-PCR cleanup was performed by adding a 1.2× volume of Solid Phase Reversible Immobilization (SPRI)-selected beads, and the libraries were incubated with beads for 5 min at RT, washed three times gently in 80% ethanol, and eluted in 22 μl of sterile ddH_2O.

ATAC sequencing

A detailed protocol for ATAC-seq is well documented, as previously described (*55*). Briefly, 50,000 cells were centrifuged at 500*g* for 5 min at RT. The cell pellet was resuspended in 50 μl of cold lysis buffer [10 mM tris-HCl (pH 7.4), 10 mM NaCl, 3 mM $MgCl_2$, and 0.1% NP-40] and centrifuged immediately at 500*g* for 10 min at 4°C. Then, the cell pellet was resuspended in 50 μl of transposase mixture (25 μl of 2× TD buffer, 22.5 μl of dH_2O, and 2.5 μl of Tn5 transposase or a final concentration of 100 nM FITC-labeled homemade Tn5) and incubated at 37°C for 30 min. After transposition, the mixture was purified with a Qiagen Mini Purification kit and eluted in 20 μl of Qiagen EB elution buffer. Sequencing libraries were prepared following the original ATAC-seq protocol. For ATAC-seq experiments after NF-YA degradation, L02 cells were treated with nocodazole for 15 hours and then treated with nocodazole and auxin for 1 hour, after which they were harvested by mitotic shake-off for ATAC-seq analysis.

Single-cell ATAC-seq

A detailed protocol for scATAC-seq using FACS is well documented, as previously described (*25*). Here, we referenced previous work on cell fixation and intranuclear staining (*56*) to sort H3pS10-positive ($H3pS10^+$) mitotic cells before Tn5 tagmentation. Briefly, cells were fixed with 1% paraformaldehyde for 10 min at RT and quenched with 0.125 M glycine for 5 min at RT. The fixed cells were then permeabilized with 0.2% NP-40 in PBS for 10 min. After regular immunostaining of H3pS10 and nuclei DNA, the Draq7/$H3pS10^+$ cells were sorted, followed by Tn5 tagmentation with 5 μl of Tn5 transposase each 50,000 cells in TD buffer [10 mM tris-HCl (pH 8.0) at 25°C, 5 mM $MgCl_2$, and 10% (v/v) *N*,*N*′-dimethylformamide]. The tagmentation reaction was done on a thermomixer (5384000039, Eppendorf) at 500 rpm and 37°C for 30 min. The reaction was then stopped by adding an equal volume of tagmentation stop buffer [10 mM tris-HCl (pH 8.0) at 25°C and 20 mM EDTA] and left on ice for 10 min. A volume of 200 μl of 1× Dulbecco's PBS with 0.5% BSA was added, and the nuclei suspension was transferred to a FACS tube. Then, single cells were sorted into plates. Each well contained 2 μl of 2× lysis

buffer [100 mM tris-HCl (pH 8.0), 100 mM NaCl, proteinase K (40 μg/ml), and 0.4% SDS] and 2 μl of primer (Ad1 and Ad2), and the plate was sealed well. The plate was put on a PCR machine, with the lid temperature set to 100°C. Then, the plate was incubated at 65°C for 15 min to release Tn5. An equal volume (4 μl) of 10% Tween 20 was then added to each well to quench SDS. Two microliters of ddH_2O and 10 μl of 2× NEB PCR Mix were added to each well, and PCR was performed with the following procedure: 72°C for 10 min; 98°C for 5 min; 22 cycles of 98°C for 10 s, 63°C for 30 s, 72°C for 1 min; 72°C for 5 min; 10°C hold. After PCR, the library was purified with a QIAquick PCR purification kit and eluted in 30 μl of Qiagen EB elution buffer. Last, the library was fragment size–selected using 0.5× SPRI upper cutoff, followed by 1.2× SPRI lower cutoff, and eluted to a final volume of 30 μl of Qiagen EB elution buffer. Sequencing libraries were prepared following the original ATAC-seq protocol.

shRNA plasmid construction and lentiviral infection

For the endogenous NF-YA gene KD experiment, shRNA sequences were inserted into the lentivirus-based PLKO.1 vector via Eco RI and Age I sites. The two following sequences target NF-YA: shNF-YA1: 5′-CCATCATGCAAGTACCTGTTT-3′, shNF-YA2: 5′-TTCTGTCCTGTAGTAAAGGGC-3′. For each sequence, the length is 21 base pairs (bp). The lentivirus-based vectors PLKO.1, psPAX2, and pMD2.G were from Addgene.

Lentivirus packaging was performed using Lipofectin-based co-transfection of human embryonic kidney (HEK) 293T cells with psPAX2, pMD2.G, and the lentiviral vector PLKO.1. The medium of the transfected cells was harvested 48 hours after transfection and filtered through a 0.22-μm filter. For infection, L02 cells were cultured in DMEM with virus at a ratio of 1:1, supplemented with polybrene (8 mg/ml) (Sigma-Aldrich), and incubated for 10 hours. Then, the culture medium was changed to DMEM containing 10% FBS followed by selection with puromycin (5 mg/liter). Forty-eight hours after selection, viable L02 cells were then maintained with puromycin (0.5 mg/liter). Compared with the negative control (shControl), shNF-YA-2 was selected for use throughout this study due to its highest KD efficiency.

Live cell imaging

Time-lapse imaging of cultured cells was accomplished with a 60× oil immersion 1.42 numerical aperture objective lens on an Olympus IX71 microscope as previously described (*57*). Images were recorded at 37°C in MatTek glass-bottom microwell dishes (MatTek) in CO_2-independent medium (Gibco) containing 10% (v/v) FBS, penicillin (100 U/ml), and streptomycin (100 μg/ml). To check chromosome dynamics in mitotic cells, images were taken for mCherry-H2B every 3 min from 24 hours after transfection. The frames were then projected with SoftWoRx software (Applied Precision) and mounted by Photoshop and Illustrator (Adobe).

5-Ethynyl-2′-deoxyuridine

The cell proliferation rate was checked with 5-Ethynyl-2′-deoxyuridine (EdU). EdU was detected with Alexa Fluor 488 azide using the Click-iT EdU Imaging Kit (C10337, Invitrogen) according to the manufacturer′s instructions. Briefly, L02 cells were treated with 10 μM EdU for 2 hours at 37°C. Then, the cells were fixed with 3.7% FA and extracted with 0.1% Triton X-100 in PBS for 10 min. After being washed three times with PBST (0.05% Tween 20 in PBS), the cells were blocked with 1% BSA (Sigma-Aldrich) in PBST for 1 hour and then incubated with Click-iT reaction cocktail for 1 hour at RT. DNA was stained with DAPI (Sigma-Aldrich).

RNA labeling and detection

Total cellular RNA was labeled for 2 hours with EU (E10345, Thermo Fisher Scientific). EU-RNA was detected with Alexa Fluor 488 azide using the Click-iT RNA Imaging Kit (C10329, Thermo Fisher Scientific) and Click-iT RNA Alexa Fluor 594 Imaging Kit (C10330, Thermo Fisher Scientific) according to the manufacturer′s instructions. In short, L02 cells were treated with 2 mM EU for 2 hours at 37°C. The cells were then fixed with 3.7% FA, followed by 0.2% Triton X-100 in PBS for the extraction step. Then, they were incubated with Click-iT reaction cocktail for 1 hour at RT. DNA was stained with DAPI (Sigma-Aldrich).

Bulk RNA-seq

Control and NF-YA KD L02 cells were synchronized with nocodazole for 16 hours and released for 80 min at 37°C. Cells were then collected and subjected to sequencing (*44*). RNA purification, reverse transcription, library construction, and sequencing were performed at Mingma Technologies Co. Ltd. in Shanghai according to the manufacturer′s instructions (Illumina). The mRNA-focused sequencing libraries from total RNA were prepared using the VAHTS mRNA-seq v3 Library Prep Kit (Vazyme). PolyA mRNA was purified from total RNA using oligo-dT–attached magnetic beads and then fragmented with fragmentation buffer. Taking these short fragments as templates, first-strand cDNA was synthesized using reverse transcriptase and random primers, followed by second-strand cDNA synthesis. Then, the synthesized cDNA was subjected to end repair, phosphorylation, and "A" base addition according to Illumina′s library construction protocol. Then, Illumina sequencing adapters were added to both sizes of the cDNA fragments. After PCR amplification for DNA enrichment, AMPure XP Beads (Beckman) were used to clean up the target fragments of 200 to 300 bp. After library construction, the Qubit 2.0 Fluorometer dsDNA HS Assay (Thermo Fisher Scientific) was used to quantify the concentration of the resulting sequencing libraries, while the size distribution was analyzed using an Agilent BioAnalyzer (Agilent). Sequencing was performed using an Illumina NovaSeq 6000 following Illumina-provided protocols for 2 × 150 paired-end sequencing at Mingma Technologies Co. Ltd. at Shanghai.

Data processing of bulk ATAC-seq

ATAC-pipe software (version 1.0.0) (*58*) (https://github.com/QuKunLab/ATAC-pipe) was used to process the raw data. We removed adapter sequences and then mapped reads to the hg19 genome assembly using Bowtie2. After removal of PCR duplicates and chrM reads, all uniquely mapped reads were shifted +4/−5 bp and then extended to 50 bp centered through the cleavage position. The reads corresponding to interphase and mitosis of each cell line were separately pooled for peak calling, with the following parameters: -f BED -g hs, -q1 0.001, -p1 1e-5, --f1 1, --pipeup 29, --nomodel, --shift 0. The open regions from three cell lines and two conditions were merged into a common open region list. Raw counts in merged open regions were quantile-normalized and $\log_2$-transformed. Bed files were converted to bedGraph files using ATAC-pipe (*58*). The ATAC-seq mean signal was then

plotted on regions of interest (bookmarked regions and unbookmarked regions) by normalizing against the ATAC-seq signal at 1000 bp upstream of the center of the regions (−1000 bp).

Analysis of published EU-RNA-seq datasets

The gene expression data during mitotic exit were collected from Palozola *et al.* (*34*) and Kang *et al.* (*19*). The expression values of multiple transcripts belonging to the same gene were averaged to obtain a unique gene-by-time expression matrix. The definition of the first wave (40′, 80′), the second wave (105′, 165′), and the third wave (300′, asynchronous) of transcriptional activation during mitotic exit is derived from Palozola's article (*34*) .

Analysis of CUT&Tag data

Raw reads were trimmed to 50 bp, adapter sequences were removed, and the trimmed sequences were aligned using Bowtie2 with the options --local --very-sensitive --no-mixed --no-discordant --phred33 -I 10 -X 700. The low-quality reads with MAPping Quality (MAPQ) < 2 were filtered out. MACS2 (*59*) was used for peak calling with the following parameters: -t target_file -c igg_file --keep-dup all --nomodel --shift 0. We used a P value of 1×10^{-12} (NF-YA) or 1×10^{-25} (NF-YB) as the threshold to select high-quality peaks. The IDR algorithm provided by the ENCODE project (v2.0.4.2) (https://www.encodeproject.org/software/idr) was used to find the reproducible binding sites between two biological replicates.

Analysis of published ATAC-seq and ChIP-seq datasets

The ATAC-seq open regions (sample $n = 181$), Pol II binding sites (sample $n = 61$) of multiple tissues/cell lines, and NF-YA binding sites of asynchronous HepG2 cells were obtained from the ENCODE database. The common Pol II binding sites were defined as those detected in at least 95% of the samples. The published ChIP-seq datasets for multiple bookmarking factors were obtained by querying the GSE number in the GEO database: GSE92846 (KLF4, H3K27ac, SOX2, and OCT4), GSE75066 (ESRRB), and GSE109962 (TBP). The retained or lost peaks for each TF and histone modification were determined by the intersection of peaks in mitotic and asynchronous cells. The datasets in other genome build will be transformed into hg19 by LiftOver (https://genome.ucsc.edu/cgi-bin/hgLiftOver).

Analysis of RNA-seq data

Raw data were aligned to hg19 through STAR. Gene expression was quantified with HTSeq (0.13.5) (https://htseq.readthedocs.io/en/master/). The DESeq2 R package (1.24) was used to normalize read counts and compute differentially expressed genes; genes with $P < 0.01$ and whose Log_2FC was either ≥ 0.5 or ≤ -0.5 were considered significant. The mean expression of a specific gene set was defined as the average expression of all genes in the set.

Acquisition of gene sets

The gene set associated with genomic stability was collected from the Harmonizome database (https://maayanlab.cloud/Harmonizome/). Gene sets associated with DNA repair, telomere maintenance, and centrosome duplication were collected from MSigDB (https://www.gsea-msigdb.org/gsea/msigdb/).

Data processing of scATAC-seq

The raw fastq data were processed by APEC (v1.1.0.11) software (*27*) (https://github.com/QuKunLab/APEC). The raw data were trimmed for adapter sequences and mapped to the hg19 genome, and PCR duplicates were removed. The uniquely mapped reads were shifted +4/−5 bp and then extended to 50 bp centered through the cleavage position. All the extended reads were pooled together for peak calling by MACS2, and the high-quality open regions with $q < 0.001$ were retained. An open region-by-cell accessibility count matrix was generated, and the proportion of reads in the open regions was calculated for each cell. Cells that had at least 1200 unique fragments and a read-in-open region ratio of 7% were kept. The original sparse cell-open region matrix was converted to a cell-accesson matrix by the APEC algorithm with the following options: ngroup = 600, npc = 40. The gene activity per cell was determined by the "APEC" gene_score function, which calculates the average normalized counts of all open regions located within ±20 kb of a gene's TSS. Functional annotation was performed by GREAT (version 3.0.0) (http://great.stanford.edu/public/html/). Genomic regions were annotated using "annotateOpen regions.pl" from the HOMER software.

Trajectory construction

The cell-accesson matrix was normalized by total count per cell and log-transformed. The low-dimensional manifold of data was calculated with "Palantir" (v1.0.0) (*60*) run_diffusion_maps (n_components = 30) and determine_multiscale_space couplings. Visualization was performed in the t-distributed stochastic neighbor embedding (tSNE) projection using the above diffusion components. Slingshot software (v1.3.2) (*28*) was used for pseudotime inference without prior knowledge.

Dynamics of chromatin accessibility during mitosis

A total of 30,671 open regions that were accessible in at least 0.5% of cells were preserved. A window containing 500 adjacent cells slid along the trajectory, with 50 cells per step, and 122 evenly sized time windows were obtained. A window-region binary matrix was obtained for the downstream analysis: If an open region was accessible in at least 1% of cells from a window, this region was defined as "open" in this window, and the corresponding element in the matrix was set to 1; otherwise, this region was defined as "closed" in this window, and the corresponding element was set to 0. The bookmarked regions were defined as open regions that were "open" in all windows, and the rest were defined as unbookmarked regions. Chromatin state characterization was performed by overlapping of the bookmarked regions with the HepG2 chromatin state annotation file, which was obtained from the UCSC website (https://genome.ucsc.edu/cgi-bin/hgFileUi?db=hg19&g=wgEncodeBroadHmm). The opening rate of each open region is defined as the number of windows where the open region is "open" divided by 122 (the total number of windows); therefore, the opening rate of the bookmarked regions was 100%. All the open regions were ranked by opening rate (from 0 to 100%) and then equally divided into 13 open chromatin bins.

Dynamics of TF binding during mitosis

For TF enrichment analysis, we first used the APEC (*27*) software to obtain the binary matrix of TF-by-open regions. The matrix element "1" means that the TF motif is found in the open region.

The TF-targeted regions were defined as the open regions containing the TF motif. Then, for a given TF_i and $window_j$, we calculated the intersection between the set of TF_i-targeted regions and the open regions that are open in $window_j$, and Fisher's exact test was used to estimate the intersection significance (*P* value). The *P* value was then adjusted to the *Q* value by Benjamini-Hochberg correction, and the enrichment score of TF_i in $window_j$ was defined as $-\log_{10}(Q \text{ value})$. Thus, an enrichment score matrix of TF-by-window was obtained by iterating the above calculation process for 241 TFs and 122 windows. The Pearson correlation coefficient (ρ) between the TF enrichment score and pseudotime in 122 windows was calculated to determine whether the TF was mitotically lost ($\rho < 0$) or mitotically enriched ($\rho > 0$). The enrichment time of a TF was defined as the pseudotime in the trajectory where the TF reached the maximum enrichment score.

Statistical analysis

All data were plotted as mean with SEM or with SD as indicated, and statistical analysis was performed with unpaired *t* test, Fisher's exact test, two-sided Wilcoxon rank-sum test, or chi-square test as indicated.

Supplementary Materials

This PDF file includes:

Figs. S1 to S8

View/request a protocol for this paper from *Bio-protocol*.

REFERENCES AND NOTES

1. F. Wang, J. M. Higgins, Histone modifications and mitosis: Countermarks, landmarks, and bookmarks. *Trends Cell Biol.* **23**, 175–184 (2013).
2. N. Naumova, M. Imakaev, G. Fudenberg, Y. Zhan, B. R. Lajoie, L. A. Mirny, J. Dekker, Organization of the mitotic chromosome. *Science* **342**, 948–953 (2013).
3. G. G. Parsons, C. A. Spencer, Mitotic repression of RNA polymerase II transcription is accompanied by release of transcription elongation complexes. *Mol. Cell. Biol.* **17**, 5791–5802 (1997).
4. M. A. Martinez-Balbas, A. Dey, S. K. Rabindran, K. Ozato, C. Wu, Displacement of sequence-specific transcription factors from mitotic chromatin. *Cell* **83**, 29–38 (1995).
5. E. Prokhortchouk, P. A. Defossez, The cell biology of DNA methylation in mammals. *Biochim. Biophys. Acta* **1783**, 2167–2173 (2008).
6. B. Pelham-Webb, A. Polyzos, L. Wojenski, A. Kloetgen, J. Li, D. C. Di Giammartino, T. Sakellaropoulos, A. Tsirigos, L. Core, E. Apostolou, H3K27ac bookmarking promotes rapid post-mitotic activation of the pluripotent stem cell program without impacting 3D chromatin reorganization. *Mol. Cell* **81**, 1732–1748.e8 (2021).
7. Y. Liu, B. Pelham-Webb, D. C. Di Giammartino, J. Li, D. Kim, K. Kita, N. Saiz, V. Garg, A. Doane, P. Giannakakou, A. K. Hadjantonakis, O. Elemento, E. Apostolou, Widespread mitotic bookmarking by histone marks and transcription factors in pluripotent stem cells. *Cell Rep.* **19**, 1283–1293 (2017).
8. C. C. Hsiung, C. S. Morrissey, M. Udugama, C. L. Frank, C. A. Keller, S. Baek, B. Giardine, G. E. Crawford, M. H. Sung, R. C. Hardison, G. A. Blobel, Genome accessibility is widely preserved and locally modulated during mitosis. *Genome Res.* **25**, 213–225 (2015).
9. M. Raccaud, E. T. Friman, A. B. Alber, H. Agarwal, C. Deluz, T. Kuhn, J. C. M. Gebhardt, D. M. Suter, Mitotic chromosome binding predicts transcription factor properties in interphase. *Nat. Commun.* **10**, 1–16 (2019).
10. C. Deluz, E. T. Friman, D. Strebinger, A. Benke, M. Raccaud, A. Callegari, M. Leleu, S. Manley, D. M. Suter, A role for mitotic bookmarking of SOX2 in pluripotency and differentiation. *Genes Dev.* **30**, 2538–2550 (2016).
11. N. Festuccia, A. Dubois, S. Vandormael-Pournin, E. Gallego Tejeda, A. Mouren, S. Bessonnard, F. Mueller, C. Proux, M. Cohen-Tannoudji, P. Navarro, Mitotic binding of Esrrb marks key regulatory regions of the pluripotency network. *Nat. Cell Biol.* **18**, 1139–1148 (2016).
12. J. M. Caravaca, G. Donahue, J. S. Becker, X. He, C. Vinson, K. S. Zaret, Bookmarking by specific and nonspecific binding of FoxA1 pioneer factor to mitotic chromosomes. *Genes Dev.* **27**, 251–260 (2013).
13. D. W. Young, M. Q. Hassan, X. Q. Yang, M. Galindo, A. Javed, S. K. Zaidi, P. Furcinitti, D. Lapointe, M. Montecino, J. B. Lian, J. L. Stein, A. J. van Wijnen, G. S. Stein, Mitotic retention of gene expression patterns by the cell fate-determining transcription factor Runx2. *Proc. Natl. Acad. Sci. U.S.A.* **104**, 3189–3194 (2007).
14. S. S. Teves, L. An, A. Bhargava-Shah, L. Xie, X. Darzacq, R. Tjian, A stable mode of bookmarking by TBP recruits RNA polymerase II to mitotic chromosomes. *eLife* **7**, e35621 (2018).
15. S. L. Klemm, Z. Shipony, W. J. Greenleaf, Chromatin accessibility and the regulatory epigenome. *Nat. Rev. Genet.* **20**, 207–220 (2019).
16. R. Zhao, T. Nakamura, Y. Fu, Z. Lazar, D. L. Spector, Gene bookmarking accelerates the kinetics of post-mitotic transcriptional re-activation. *Nat. Cell Biol.* **13**, 1295–1304 (2011).
17. S. K. Zaidi, D. W. Young, M. A. Montecino, J. B. Lian, A. J. van Wijnen, J. L. Stein, G. S. Stein, Mitotic bookmarking of genes: A novel dimension to epigenetic control. *Nat. Rev. Genet.* **11**, 583–589 (2010).
18. H. Zhang, D. J. Emerson, T. G. Gilgenast, K. R. Titus, Y. Lan, P. Huang, D. Zhang, H. Wang, C. A. Keller, B. Giardine, R. C. Hardison, J. E. Phillips-Cremins, G. A. Blobel, Chromatin structure dynamics during the mitosis-to-G1 phase transition. *Nature* **576**, 158–162 (2019).
19. H. Kang, M. N. Shokhirev, Z. Xu, S. Chandran, J. R. Dixon, M. W. Hetzer, Dynamic regulation of histone modifications and long-range chromosomal interactions during postmitotic transcriptional reactivation. *Genes Dev.* **34**, 913–930 (2020).
20. S. Gandhi, R. Mitterhoff, R. Rapoport, M. Farago, A. Greenberg, L. Hodge, S. Eden, C. Benner, A. Goren, I. Simon, Mitotic H3K9ac is controlled by phase-specific activity of HDAC2, HDAC3, and SIRT1. *Life Sci. Alliance* **5**, e202201433 (2022).
21. N. Festuccia, I. Gonzalez, N. Owens, P. Navarro, Mitotic bookmarking in development and stem cells. *Development* **144**, 3633–3645 (2017).
22. T. Nagano, Y. Lubling, C. Varnai, C. Dudley, W. Leung, Y. Baran, N. Mendelson Cohen, S. Wingett, P. Fraser, A. Tanay, Cell-cycle dynamics of chromosomal organization at single-cell resolution. *Nature* **547**, 61–67 (2017).
23. J. Karlsson, T. Kroneis, E. Jonasson, E. Larsson, A. Stahlberg, Transcriptomic characterization of the human cell cycle in individual unsynchronized cells. *J. Mol. Biol.* **429**, 3909–3924 (2017).
24. D. Mahdessian, A. J. Cesnik, C. Gnann, F. Danielsson, L. Stenstrom, M. Arif, C. Zhang, T. Le, F. Johansson, R. Shutten, A. Backstrom, U. Axelsson, P. Thul, N. H. Cho, O. Carja, M. Uhlen, A. Mardinoglu, C. Stadler, C. Lindskog, B. Ayoglu, M. D. Leonetti, F. Ponten, D. P. Sullivan, E. Lundberg, Spatiotemporal dissection of the cell cycle with single-cell proteogenomics. *Nature* **590**, 649–654 (2021).
25. X. Chen, R. J. Miragaia, K. N. Natarajan, S. A. Teichmann, A rapid and robust method for single cell chromatin accessibility profiling. *Nat. Commun.* **9**, 1–9 (2018).
26. T. Hirota, J. J. Lipp, B. H. Toh, J. M. Peters, Histone H3 serine 10 phosphorylation by Aurora B causes HP1 dissociation from heterochromatin. *Nature* **438**, 1176–1180 (2005).
27. B. Li, Y. Li, K. Li, L. Zhu, Q. Yu, P. Cai, J. Fang, W. Zhang, P. Du, C. Jiang, J. Lin, K. Qu, APEC: An accesson-based method for single-cell chromatin accessibility analysis. *Genome Biol.* **21**, 1–27 (2020).
28. K. Street, D. Risso, R. B. Fletcher, D. Das, J. Ngai, N. Yosef, E. Purdom, S. Dudoit, Slingshot: Cell lineage and pseudotime inference for single-cell transcriptomics. *BMC Genomics* **19**, 1–16 (2018).
29. L. Krenning, S. Sonneveld, M. Tanenbaum, Time-resolved single-cell sequencing identifies multiple waves of mRNA decay during the mitosis-to-G1 phase transition. *eLife* **11**, e71356 (2022).
30. K. Wang, B. Sturt-Gillespie, J. C. Hittle, D. Macdonald, G. K. Chan, T. J. Yen, S. T. Liu, Thyroid hormone receptor interacting protein 13 (TRIP13) AAA-ATPase is a novel mitotic checkpoint-silencing protein. *J. Biol. Chem.* **289**, 23928–23937 (2014).
31. X. Chen, Y. Shen, W. Draper, J. D. Buenrostro, U. Litzenburger, S. W. Cho, A. T. Satpathy, A. C. Carter, R. P. Ghosh, A. East-Seletsky, J. A. Doudna, W. J. Greenleaf, J. T. Liphardt, H. Y. Chang, ATAC-see reveals the accessible genome by transposase-mediated imaging and sequencing. *Nat. Methods* **13**, 1013–1020 (2016).
32. C. Trapnell, D. Cacchiarelli, J. Grimsby, P. Pokharel, S. Li, M. Morse, N. J. Lennon, K. J. Livak, T. S. Mikkelsen, J. L. Rinn, The dynamics and regulators of cell fate decisions are revealed by pseudotemporal ordering of single cells. *Nat. Biotechnol.* **32**, 381–386 (2014).
33. C. Y. McLean, D. Bristor, M. Hiller, S. L. Clarke, B. T. Schaar, C. B. Lowe, A. M. Wenger, G. Bejerano, GREAT improves functional interpretation of cis-regulatory regions. *Nat. Biotechnol.* **28**, 495–501 (2010).
34. K. C. Palozola, G. Donahue, H. Liu, G. R. Grant, J. S. Becker, A. Cote, H. Yu, A. Raj, K. S. Zaret, Mitotic transcription and waves of gene reactivation during mitotic exit. *Science* **358**, 119–122 (2017).

35. M. A. F. Soares, D. S. Soares, V. Teixeira, A. Heskol, R. B. Bressan, S. M. Pollard, R. A. Oliveira, D. S. Castro, Hierarchical reactivation of transcription during mitosis-to-G1 transition by Brn2 and Ascl1 in neural stem cells. *Genes Dev.* **35**, 1020–1034 (2021).
36. S. Kadauke, G. A. Blobel, Mitotic bookmarking by transcription factors. *Epigenetics Chromatin* **6**, 1–10 (2013).
37. J. Yang, E. Sung, P. G. Donlin-Asp, V. G. Corces, A subset of Drosophila Myc sites remain associated with mitotic chromosomes colocalized with insulator proteins. *Nat. Commun.* **4**, 1–9 (2013).
38. L. E. Greenbaum, W. Li, D. E. Cressman, Y. Peng, G. Ciliberto, V. Poli, R. Taub, CCAAT enhancer-binding protein beta is required for normal hepatocyte proliferation in mice after partial hepatectomy. *J. Clin. Invest.* **102**, 996–1007 (1998).
39. E. Stepniak, R. Ricci, R. Eferl, G. Sumara, I. Sumara, M. Rath, L. Hui, E. F. Wagner, c-Jun/AP-1 controls liver regeneration by repressing p53/p21 and p38 MAPK activity. *Genes Dev.* **20**, 2306–2314 (2006).
40. M. Nardini, N. Gnesutta, G. Donati, R. Gatta, C. Forni, A. Fossati, C. Vonrhein, D. Moras, C. Romier, M. Bolognesi, R. Mantovani, Sequence-specific transcription factor NF-Y displays histone-like DNA binding and H2B-like ubiquitination. *Cell* **152**, 132–143 (2013).
41. X. Liu, L. Xu, J. Li, P. Y. Yao, W. Wang, H. Ismail, H. Wang, B. Liao, Z. Yang, T. Ward, K. Ruan, J. Zhang, Q. Wu, P. He, X. Ding, D. Wang, C. Fu, Z. Dou, F. Yan, W. Wang, X. Liu, X. Yao, Mitotic motor CENP-E cooperates with PRC1 in temporal control of central spindle assembly. *J. Mol. Cell Biol.* **12**, 654–665 (2020).
42. P. Arampatzi, M. Gialitakis, T. Makatounakis, J. Papamatheakis, Gene-specific factors determine mitotic expression and bookmarking via alternate regulatory elements. *Nucleic Acids Res.* **41**, 2202–2215 (2013).
43. P. Benatti, D. Dolfini, A. Vigano, M. Ravo, A. Weisz, C. Imbriano, Specific inhibition of NF-Y subunits triggers different cell proliferation defects. *Nucleic Acids Res.* **39**, 5356–5368 (2011).
44. Z. M. Lai, W. R. Shan, J. Li, J. Min, X. Z. Zeng, Z. Y. Zuo, Appropriate exercise level attenuates gut dysbiosis and valeric acid increase to improve neuroplasticity and cognitive function after surgery in mice. *Mol. Psychiatry* **26**, 7167–7187 (2021).
45. M. Fenech, M. Kirsch-Volders, A. T. Natarajan, J. Surralles, J. W. Crott, J. Parry, H. Norppa, D. A. Eastmond, J. D. Tucker, P. Thomas, Molecular mechanisms of micronucleus, nucleoplasmic bridge and nuclear bud formation in mammalian and human cells. *Mutagenesis* **26**, 125–132 (2011).
46. M. Terradas, M. Martin, L. Tusell, A. Genesca, Genetic activities in micronuclei: Is the DNA entrapped in micronuclei lost for the cell? *Mutat. Res.* **705**, 60–67 (2010).
47. T. Natsume, T. Kiyomitsu, Y. Saga, M. T. Kanemaki, Rapid protein depletion in human cells by auxin-inducible degron tagging with short homology donors. *Cell Rep.* **15**, 210–218 (2016).
48. K. C. Palozola, J. Lerner, K. S. Zaret, A changing paradigm of transcriptional memory propagation through mitosis. *Nat. Rev. Mol. Cell Biol.* **20**, 55–64 (2018).
49. R. P. Halley-Stott, J. Jullien, V. Pasque, J. Gurdon, Mitosis gives a brief window of opportunity for a change in gene transcription. *PLOS Biol.* **12**, e1001914 (2014).
50. D. Egli, J. Rosains, G. Birkhoff, K. Eggan, Developmental reprogramming after chromosome transfer into mitotic mouse zygotes. *Nature* **447**, 679–685 (2007).
51. F. Lu, Y. Liu, A. Inoue, T. Suzuki, K. Zhao, Y. Zhang, Establishing chromatin regulatory landscape during mouse preimplantation development. *Cell* **165**, 1375–1388 (2016).
52. A. J. Oldfield, P. Yang, A. E. Conway, S. Cinghu, J. M. Freudenberg, S. Yellaboina, R. Jothi, Histone-fold domain protein NF-Y promotes chromatin accessibility for cell type-specific master transcription factors. *Mol. Cell* **55**, 708–722 (2014).
53. A. J. Oldfield, T. Henriques, D. Kumar, A. B. Burkholder, S. Cinghu, D. Paulet, B. D. Bennett, P. Yang, B. S. Scruggs, C. A. Lavender, E. Rivals, K. Adelman, R. Jothi, NF-Y controls fidelity of transcription initiation at gene promoters through maintenance of the nucleosome-depleted region. *Nat. Commun.* **10**, 1–12 (2019).
54. P. Xia, X. Liu, B. Wu, S. Zhang, X. Song, P. Y. Yao, J. Lippincott-Schwartz, X. Yao, Superresolution imaging reveals structural features of EB1 in microtubule plus-end tracking. *Mol. Biol. Cell* **25**, 4166–4173 (2014).
55. J. D. Buenrostro, P. G. Giresi, L. C. Zaba, H. Y. Chang, W. J. Greenleaf, Transposition of native chromatin for fast and sensitive epigenomic profiling of open chromatin, DNA-binding proteins and nucleosome position. *Nat. Methods* **10**, 1213–1218 (2013).
56. X. Chen, U. M. Litzenburger, Y. Wei, A. N. Schep, E. L. LaGory, H. Choudhry, A. J. Giaccia, W. J. Greenleaf, H. Y. Chang, Joint single-cell DNA accessibility and protein epitope profiling reveals environmental regulation of epigenomic heterogeneity. *Nat. Commun.* **9**, 1–12 (2018).
57. P. Xia, Z. K. Wang, X. Liu, B. Wu, J. C. Wang, T. Ward, L. Y. Zhang, X. Ding, G. Gibbons, Y. Y. Shi, X. B. Yao, EB1 acetylation by P300/CBP-associated factor (PCAF) ensures accurate kinetochore-microtubule interactions in mitosis. *Proc. Natl. Acad. Sci. U.S.A.* **109**, 16564–16569 (2012).
58. Z. Zuo, Y. Jin, W. Zhang, Y. Lu, B. Li, K. Qu, ATAC-pipe: General analysis of genome-wide chromatin accessibility. *Brief. Bioinform.* **20**, 1934–1943 (2019).
59. Y. Zhang, T. Liu, C. A. Meyer, J. Eeckhoute, D. S. Johnson, B. E. Bernstein, C. Nusbaum, R. M. Myers, M. Brown, W. Li, X. S. Liu, Model-based analysis of ChIP-Seq (MACS). *Genome Biol.* **9**, 1–9 (2008).
60. M. Setty, V. Kiseliovas, J. Levine, A. Gayoso, L. Mazutis, D. Pe'er, Characterization of cell fate probabilities in single-cell data with Palantir. *Nat. Biotechnol.* **37**, 451–460 (2019).

Acknowledgments: We thank all members in the Qu and Yao laboratories for helpful discussions. We are grateful for the gift of L02 cells from C. Li of Nanjing University and special thanks to X. Yao for constructive suggestions. We thank the USTC supercomputing center and the School of Life Science Bioinformatics Center for providing computing resources for this project. **Funding:** This work was supported by the National Key R&D Program of China (2020YFA0112200 and 2022YFA1303200 to K.Q.), the National Natural Science Foundation of China (T2125012, 91940306, 31970858, and 31771428 to K.Q.; 32100457 to J.F.; 32090040, 91854203, 31621002, 91853115, and 32100612 to X.L.; 22177106 to X.Y.; and 32270978 to C.G.), the Fundamental Research Funds for the Central Universities (YD2070002019, WK9110000141, and WK2070000158 to K.Q.), the Youth Innovation Fund of University of Science and Technology of China (WK9100000018 to J.F.), the National Key R&D Program of China (2022YFA1303100 and 2022YFA1302700 to Z.W.), . **Author contributions:** K.Q. conceived the project. Q.Y., X.L., J.F., and H.W. designed experiments. X.L., H.W., Q.S., and Z.W. performed experiments with help from C.G. and X.Y. Q.Y. and J.F. performed computational analyses with help from W.Z., N.L., and C.J. K.Q. and Z.W. supervised the project. K.Q., Q.Y., and Z.W. wrote the manuscript with inputs from all authors. All authors read and approved the final manuscript. **Competing interests:** J.F. is the chief executive officer of HanGen Biotech. The other authors declare that they have no competing interests. **Data and materials availability:** All data needed to evaluate the conclusions in the paper are present in the paper and/or the Supplementary Materials. Raw sequencing data are deposited to Genome Sequence Archive (GSA) under the accession number CRA003844. The source code is available at GitHub (https://github.com/QuKunLab/Mitosis) and Zenodo (https://doi.org/10.5281/zenodo.7313683).

Submitted 28 May 2022
Accepted 29 December 2022
Published 25 January 2023
10.1126/sciadv.add2175

ScienceAdvances

Dynamics and regulation of mitotic chromatin accessibility bookmarking at single-cell resolution

Qiaoni Yu, Xu Liu, Jingwen Fang, Huihui Wu, Chuang Guo, Wen Zhang, Nianping Liu, Chen Jiang, Qing Sha, Xiao Yuan, Zhikai Wang, and Kun Qu

Sci. Adv., **9** (4), eadd2175.
DOI: 10.1126/sciadv.add2175

Science Advances (ISSN) is published by the American Association for the Advancement of Science. 1200 New York Avenue NW, Washington, DC 20005. The title *Science Advances* is a registered trademark of AAAS.